Cascade in muonic deuterium atoms

B. Lauss,* P. Ackerbauer, W. H. Breunlich, B. Gartner, M. Jeitler,† P. Kammel,‡ J. Marton, W. Prymas, and J. Zmeskal
Institute for Medium Energy Physics, Austrian Academy of Sciences, Boltzmanngasse 3, A-1090 Wien, Austria

D. Chatellard and J.-P. Egger
Institut de Physique de l'Université, CH-2000 Neuchâtel, Switzerland

H. Daniel, F. J. Hartmann, and A. Kosak
Physics Department, TU München, D-85747 Garching, Germany

C. Petitjean
Paul Scherrer Institut, CH-5232 Villigen, Switzerland
(Received 12 June 1998)

The cascade in muonic deuterium atoms has been investigated experimentally, employing deeply depleted charge-coupled devices as x-ray detectors. The relative x-ray yields for the muonic deuterium transitions $K\alpha$, $K\beta$, and $K\gamma$ and the $K\alpha/K\beta$ ratios have been measured at densities between 0.0107 and 1.145 of liquid-hydrogen density. The results are compared with our measurements of the muonic x rays in hydrogen and in liquid-hydrogen deuterium mixtures in search for an isotopic effect. A comparison of our results with recent calculations is given. [S1050-2947(99)06906-1]

PACS number(s): 36.10.Dr, 32.30.Rj, 32.70.Fw

I. INTRODUCTION

Observing the photons emitted during the deexcitation of a muonic atom allows us to test our view of exotic atoms and helps us to understand the complex chain of deexcitation processes, the so-called muonic cascade [1–7].

Due to the muon's mass, which is ~207 times the electron mass, the μd atom is much smaller than an ordinary deuterium atom and its energy levels are much deeper. While UV light is emitted in transitions to the ground state of ordinary deuterium (K series—$K\alpha$, $K\beta$, $K\gamma,\ldots$), the corresponding muonic transitions proceed via the emission of x rays with an energy of ~2 keV.

Three main reasons motivated the present measurements.

(i) In an earlier experiment [8] we have measured the x rays emitted during the cascade in muonic hydrogen. The observed x-ray yields and $K\alpha/K\beta$ ratios were in rough agreement with the existing calculations, but the comparison with a recent Monte-Carlo cascade calculation [6] showed puzzling inconsistencies with respect to the influence of Coulomb deexcitation (see Sec. II). The observed contribution of this process and its effect on the density dependence of the $K\alpha/K\beta$ ratios do not correspond to the predictions of this calculation. As Coulomb deexcitation is thought to contribute significantly to the cascade only in hydrogen isotopes, we wanted to confirm the importance of this process with a measurement of the muonic cascade in deuterium. Other x-ray experiments [9–13] were not accurate or sensitive enough to clarify this question.

(ii) We also wanted to look for an isotopic effect in the x-ray yields and $K\alpha/K\beta$ ratios. Regarding the yields, theory predicts a difference of only a few percent between muonic hydrogen and the heavier isotope, deuterium; the difference expected in the $K\alpha/K\beta$ ratios is up to ~20% at liquid hydrogen density (LHD).[1] This prediction needed to be checked experimentally.

The search for an isotopic effect is also motivated by muon-catalyzed fusion (μCF). The muonic cascade sets the initial conditions for μCF in hydrogen isotopes [14–17]. Due to the high efficiency of the catalysis process, deuterium-tritium mixtures are of special interest. The understanding of isotopic effects in the atomic cascades of hydrogen and deuterium is especially important for the prediction of the cascade processes in muonic tritium atoms, where experimental investigations are still lacking and are very difficult. Also, the understanding of the process of excited state muon transfer in mixtures of hydrogen isotopes [18], important in μCF kinetics, requires the knowledge of the cascade in pure H_2, D_2, and T_2 as a prerequisite.

(iii) The accuracy of the determination of the strong interaction width of the energy levels in pionic deuterium ($\pi^- d$), which is directly correlated to the pion-nucleon scattering length, is restricted by Doppler broadening of the x-ray peaks, mainly caused by Coulomb deexcitation [19,20]. The muonic cascade, unaffected by the strong interaction, may be used as a probe for the atomic deexcitation processes in $\pi^- d$, which are thought to be comparable except for the pion's nuclear absorption due to the strong interaction, which starts already at energy levels as high as $n=5$.

*Electronic address: lauss@amuon.imep.univie.ac.at
†Present address: CERN/EP, CH-1211 Geneva 23, Switzerland.
‡Present address: University of California and L. Berkeley National Laboratory, Berkeley, CA 94720.

[1]Liquid-hydrogen density (LHD)=4.25×10^{22} atoms/cm^3.

We have performed a series of measurements to investigate the muonic cascade in hydrogen isotopes. In the present paper the experimental method is discussed in detail, new results for gaseous and liquid deuterium are presented, and these results are compared with measurements in pure hydrogen [8] and with new results in liquid hydrogen deuterium mixtures.

II. BRIEF SKETCH OF THE PRESENT THEORETICAL PICTURE

When slowed down in a deuterium target, a muon can form a μd atom via Coulomb capture by replacing the electron of the deuterium atom [1,21]. This leaves the muon most likely in an initial state of $11 \leqslant n \leqslant 15$ [22]. Rapid deexcitation follows, ending with the muon in the $1s$ state, where it can either decay or interact weakly with the nucleus [23].

The muonic cascade proceeds via a competition of different collisional processes and emission of radiation. As the μd atom is small and has no electric charge, it can penetrate deeply into the electron cloud of neighboring atoms and molecules, where it is exposed to the strong inneratomic electromagnetic fields of nuclei and electrons. The electric fields can induce transitions of the muon to the next lower energy level $(n-1)$ (Coulomb deexcitation) [1] or between states of various orbital angular momenta l (Stark mixing) [1].

Coulomb deexcitation is possible if the energy of the interaction is comparable to the level spacing, in which case induced transitions, predominately to the next lower level, can occur [24]. The transition energy is directly transferred to the kinetic energy of the collision partners. According to Markushin [5,6], the muonic atom can be accelerated up to epithermal energies of ~ 200 eV, which is equivalent to a temperature of more than one million degrees. This is the only known cascade process which can accelerate an exotic atom to such high energies. Coulomb deexcitation is expected to cause up to 40% of μd atoms in the ground state to have energies above 50 eV [5]. Deceleration due to elastic scattering is too slow to thermalize all μd atoms during the cascade. Recent experiments on the muonic and pionic cascade in hydrogen [8,18,25–27] have demonstrated the importance of Coulomb deexcitation but this cascade process is still considered the least known one [6]. Existing calculations of the Coulomb deexcitation cross sections differ among themselves by more than one order of magnitude [24,28–31]. Coulomb deexcitation is believed to contribute significantly only to the muonic cascade of hydrogen isotopes, while Stark mixing is important in the cascade of various light atoms.

Stark mixing is caused by the electric fields of surrounding nuclei [1,32]. These fields can induce rapid oscillations between all degenerate l sublevels of the μd atom. For our experimental conditions, the corresponding rates are large compared to other cascade processes [5,6]. This guarantees a statistical population of the various l sublevels at all stages. In the investigated density region our observables are not sensitive to a small variation of the Stark mixing cross sections [2,5].

Another important collisional cascade process is due to the external Auger effect. This effect designates the transmission of the transition energy to an electron of a neighboring atom or molecule, which then is ionized. At our experimental conditions the external Auger effect dominates the cascade at $n \sim 7$, because at this stage even a $\Delta n = 1$ transition releases the energy necessary for ionization [7].

Competing with all collisional processes are radiative transitions. These transition rates do not depend on density or collision energy and can be calculated very accurately [4,5]. The μd atom gains (nearly) no kinetic energy in radiative transitions. As x rays can be readily detected, this is the most important process from our experimental point of view.

All of the above processes, except Coulomb deexcitation, are considered in the ''standard cascade model'' [1–4,7,33] which has another severe limitation: it does not take into account the change of the kinetic energy $\epsilon_{\mu d}$ of the μd atom during the cascade. This is important because the rates of all collisional cascade processes are energy dependent. Recent Monte Carlo calculations of the cascade in muonic hydrogen and muonic deuterium [5,6] try to take into account the time evolution of the kinetic energy of the muonic atom for energy levels $n \leqslant 6$. This results in a complex distribution of $\epsilon_{\mu d}$ at various stages. This calculation also tries to express the lack of understanding of the real Coulomb deexcitation rates by scaling the corresponding cross sections taken from Bracci and Fiorentini [24] by a factor k: $k=0$ corresponds to no influence of Coulomb deexcitation as in the standard casacade model; $k=1$ means the cross sections from Ref. [24] are correct. The understanding of Coulomb deexcitation enables a reliable calculation of the energy distribution of the μd atoms in the ground and some excited states.

As all of the effective collisional rates obviously scale with density, one can influence the competition between radiation and collisional processes by selecting specific target conditions. In the density region observed in our experiment, viz. 0.0107 to 1.145 of LHD, the transitions to the ground state are strongly dominated by x-ray emission: at gas densities theory expects these transitions to proceed practically always via x-ray emission; at LHD the probability for x-ray emission is still ~ 95 % [2,5,6].

A measurement of the x-ray yields tests the rates of the collisional processes considered in the cascade model; the $K\alpha/K\beta$ ratio tests the model at the energy level $n=3$, where the competition between radiative transitions $3 \rightarrow 1$ and collisional transitions $3 \rightarrow 2$ followed immediately by $K\alpha$ x rays takes place. As the Auger deexcitation rates are believed to be well known [6,34], this ratio can be regarded as a direct test of the Coulomb deexcitation rates.

III. THE EXPERIMENT

A. Setup

The main observables in this experiment were the x rays originating from the $2 \rightarrow 1$, $3 \rightarrow 1$, and $4 \rightarrow 1$ transitions in muonic deuterium. Their corresponding energies are calculated to be about 2.00 keV ($K\alpha$), 2.37 keV ($K\beta$), and 2.50 keV ($K\gamma$).

We used the high-intensity muon beam of the $\mu E4$ area at PSI (Paul Scherrer Institute, Villigen, Switzerland) for our measurements. The μ-beam momentum was set to ~ 40 MeV/c for measurements at LHD and between

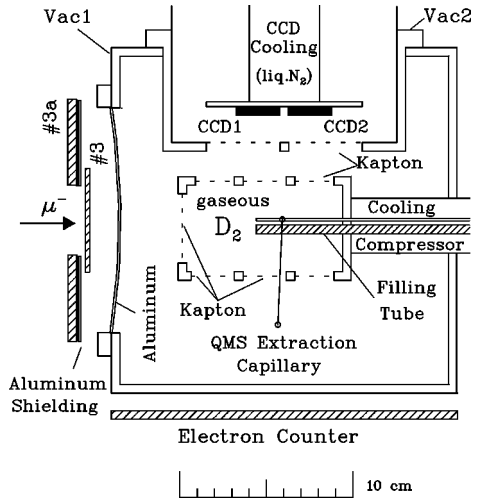

FIG. 1. Top view of the setup of the experiment. The displayed target cell was used for measurements of gaseous deuterium. The filling tube and extraction capillary were fixed outside the cell. The filling and extraction opening was in the center of the upper target cell wall. Two separated vacuum vessels were used: one for the target (Vac1), and one for the CCD detector (Vac2). The scintillation counter telescope 3, $\overline{3a}$ was used to detect incoming muons, the electron counter to detect electrons following muon decay; both were necessary to ensure an optimum stopping efficiency. A smaller target cell, adapted to the expected extent of the muon stopping distributions, was used for the measurements at LHD [18].

28 MeV/c and 35 MeV/c for gas targets. This caused different muon stopping distributions at various target densities centered in the middle of the target cell. The corresponding widths [full width at half maximum (FWHM)] of these distributions in the beam direction were $\sim$4 mm for LHD and $\sim$20 mm–100 mm for gas targets.

The experimental setup is shown in Fig. 1. Incoming negative muons were identified by a telescope of plastic scintillation counters, viz., counter 3, with 3a in anticoincidence mode, and brought to rest in deuterium contained in a silver-coated steel or aluminum target cell. Adapted to the expected muon stopping distributions, the box-shaped target cells had a length of 34 mm in the beam direction for liquid deuterium and 95 mm or 110 mm for gas and a square shape perpendicular to the beam with a side length of 40 mm for liquid and 65 mm for gas measurements.

Kapton and Hostaphan foils with a thickness of 12.5 μm (for the measurements at LHD) and 25 μm or 36 μm (gaseous targets) were used as window materials to withstand temperatures around 20 K (the target cell had to endure several cooling cycles) and gas pressures up to 6 bar. To reduce radiation heating, superinsulation partly covered the target cell contained in an insulation vacuum jacket made of stainless steel. An additional 12.5 μm Kapton window separated the target vacuum vessel from the detector vacuum.

A closed-loop helium compressor system was used to cool the target cells to temperatures between 20 and 35 K. Temperature and pressure of the target were monitored and controlled during all the runs.

The D_2 gas was filled directly into the target cell via a palladium filter and a liquid-nitrogen trap to reduce $Z \geqslant 2$ contamination to less than 10 ppm. High-Z materials would induce excited state muon transfer and change the specific intensity pattern of the K lines [18,35,36]. Gas samples were taken directly out of the target cell during all measurements and checked for impurities with a quadrupole mass-spectrometry system (QMS) [37].

A Monte Carlo simulation of our setup showed a negligible number of muon stops close to the target walls and windows. Thus excited state transfer to wall materials should be negligible for our measurements. This was confirmed by a monitoring Ge-diode detector, which did not observe delayed (with respect to the muon stop) muonic aluminum x rays at a level higher than 0.1% of the prompt μ stops. Prompt μAl x rays are due to muons directly stopping in the target cell walls; delayed Al x rays are caused by muons, which, after the μd atom drifts to the wall, transfer to the aluminum atoms.

The electron counter was used to measure the electrons originating from muon decay in deuterium. The corresponding characteristic lifetime of $\tau_0 \sim 2.2$ μs was observed. The relative intensity of decay electrons was used to tune the muon momentum for an optimal stopping position.

B. X-ray detector

For this measurement we used charge coupled devices (CCDs) as an x-ray detector [38–41]. The detector consisted of two independent, deeply depleted CCD chips[2] each having an active detection area of $\sim 25 \times 17$ mm^2 ($\sim$880 000 pixels) and a depletion thickness of $\sim$30 μm. The pixel size is 22.5 μm$\times$22.5 μm. The material of the chip was mainly silicon with small absorption layers of SiO_2 and Si_3N_4 on the surface.

Electronically, each chip was split into two halves to shorten the readout time to $\sim$28 s. This slow readout guaranteed an energy resolution of $\Delta E_{FWHM} \sim 6\%$ at 2 keV; faster readout would have resulted in a lower pixel transfer efficiency [42].

Liquid nitrogen was used to cool the CCD sensors to $\sim$160 K by using a copper rod as a thermal connector. This resulted in a drastic reduction of the thermal noise.

Due to the specific interaction characteristics of x rays in our detector, we were able to apply a pattern recognition algorithm to separate ''true'' x-ray hits from charged particles using a ''single pixel'' selection criterion [40–43]. A ''single pixel'' was considered to be a ''true'' x ray if the charge content of the surrounding eight neighbor pixels were statistically compatible with the noise peak of the CCDs. This was checked via the distributions of the mean and maximum energy deposited in the neighboring pixels and of their standard deviations [42–45]. For the case of a ''true'' x ray these three distributions reflect the respective noise peak distributions.

Depending on the absolute beam intensity, CCD exposures lasted on the average three minutes. All hits in this time interval were recorded as one exposure. Not more than $\sim$15% of the CCDs' pixels were allowed to be hit, otherwise the detection efficiency would have been decreased severely.

[2]Type CCD-05-20-207 by EEV (English Electric Valve), Waterhouse Lane, Chelmsford, Essex, England.

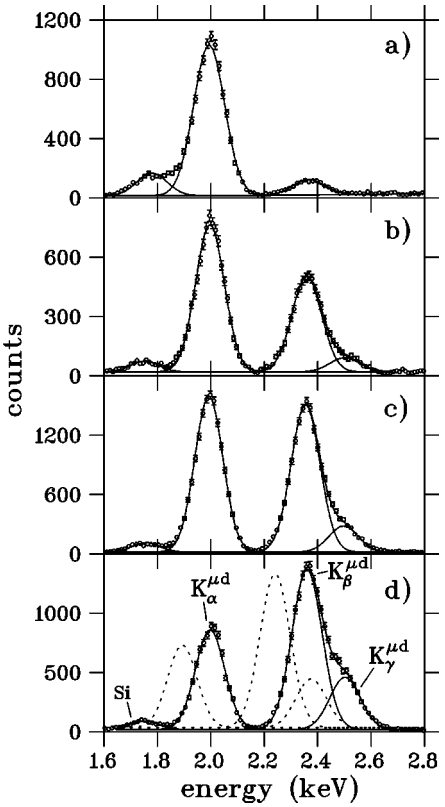

FIG. 2. Energy spectra of muonic x rays observed in deuterium at various target densities Φ (given in units of LHD): (a) $\Phi = 1.145$, (b) $\Phi = 0.0783$, (c) $\Phi = 0.0399$, (d) $\Phi = 0.0133$. The lines corresponding to the $K_\alpha^{\mu d}$, $K_\beta^{\mu d}$, and $K_\gamma^{\mu d}$ transitions are separated. The solid lines indicate Gaussian fits. The density dependence of the line intensities is clearly visible. The x-ray peak at 1.74 keV is due to fluorescence excitation of the detector's silicon material. The isotopic energy shift compared to muonic hydrogen is demonstrated in (d), where the dotted lines display the corresponding $K^{\mu p}$ lines which were observed in muonic hydrogen [8].

More than 40% pixel hits would have made it very difficult to apply our pattern recognition algorithm.

Some of the energy spectra are displayed in Fig. 2. The target density is decreasing from (a) to (d). One can clearly see the density dependence of the individual line yields, especially the dramatic rise of the $K\beta$ line with decreasing density. The radiative $4 \rightarrow 1$ transition seems to be relevant only at gas densities, because with increasing density collisional processes obviously dominate over x-ray emission. No significant contribution from K lines higher than $K\gamma$ has been observed. Figure 2(d) also shows the observed isotopic energy shift of the $K^{\mu d}$ lines compared to the $K^{\mu p}$ peaks (dotted lines). The x-ray peak at 1.74 keV is due to fluorescence excitation of the detector's silicon material.

IV. DATA ANALYSIS AND RESULTS

A. Determination of the detection efficiency

The knowledge of the relative difference of the x-ray detection efficiency at the various K series energies was essential for our analysis. Therefore all x-ray absorbers between the places of origin and of detection of the x rays had to be known precisely. A Monte Carlo simulation program was written to account for all relevant effects [46].

(i) We used the GEANT simulation package [47] to calculate the muon stopping distributions in the respective targets. The stopping point of the muon in the target deuterium was considered to be the origin of the cascade x rays. The center of the stopping distribution coincided with the center of the target cell. Changing the stopping center by ± 3 cm (± 1 cm for measurements at LHD) in the beam direction and by ± 1 cm in both perpendicular directions caused different effective thicknesses of the absorbers (e.g., the path length in deuterium strongly depends on the stopping center). This allowed us to estimate this particular contribution to the uncertainty of the detection efficiency.

(ii) The high gas pressure inside the target cell caused the windows to bulge. Before and after operation, the exact thicknesses of the windows were measured to an accuracy of ~ 1 μm. Because of the small thermal expansion coefficient of the window materials, we considered the shape and thicknesses measured at room temperature to reflect those at experimental conditions. The calculation of the x-ray absorption in Kapton and in Hostaphan was checked experimentally by measuring the x-ray absorption in foils of different thickness [44]. This was done with a Ge-diode detector and a ^{55}Fe-source to a precision better than 5%.

(iii) The exact shape of the respective target cell and the convex shape of its windows was simulated. This was considered to introduce an additional error of ± 1 μm for the window thicknesses.

(iv) The x-ray absorption in deuterium was calculated between the point of origin of the x ray and the windows of the respective target cell.

(v) The individual absorption layers of the CCD chips were simulated according to the production thicknesses [48]. The intrinsic absorption efficiency was checked experimentally at the 10% level by measuring the known intensity ratios of electronic x-ray lines in the region 1–10 keV [49] and of antiprotonic nitrogen and oxygen x rays at very low gas densities [44,50]. At such densities x-ray transitions at high n levels were shown to have equal intensities [51]. Hence the measured line intensities directly reflect the detector efficiency. The actual thickness of the depletion region was assumed to be 30 μm. Its exact value was of minor importance for the efficiency evaluation in the 2 keV region.

(vi) We used the x-ray-absorption coefficients given in Ref. [52]. For the exact absorption behavior of silicon and silicon compounds we have used the results of [53,54] which measured the x-ray absorption of similar CCDs produced by EEV. The x-ray-absorption fine structure (XAFS) was taken into account. The error of the absorption coefficients, which is not given in Ref. [52], was estimated to be $\sim 5\%$ by comparison with the calculations of Refs. [55,56].

In Fig. 3(a) the calculated energy dependence of the detection efficiency and the contributions of the various absorbers are displayed for the measurement at a density of 4% of LHD. The dotted lines show the estimated 1σ error bands. Figure 3(b) shows the efficiencies for various setups.

It should be emphasized that only the efficiency ratios (relative efficiencies) $\eta(K\alpha)/\eta(K\beta)$ and $\eta(K\alpha)/\eta(K\gamma)$ are needed in the analysis [$\eta(K_i)$ denotes the efficiency at the energy of the respective K_i x-ray peak]. The error of the efficiency calculation was evaluated by using minimum and maximum thicknesses of the different absorbers, measured

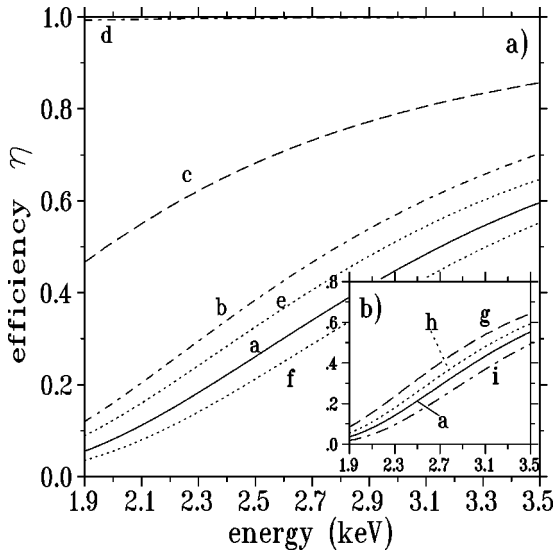

FIG. 3. The calculated energy dependence of the x-ray detection efficiency. The solid angle of the active detection area of the CCDs is neglected. (a) Detection efficiency for the measurement at $\Phi = 4\%$ of LHD (a, full line). It is the product of the given contributions due to absorption in the windows (b, dashed-dotted line), absorption in the CCD top layers (c, dashed line), and absorption in the deuterium gas (d, dashed-dotted line). A variation of the depletion thickness between 15 and 50 μm does not affect the efficiency in the relevant energy region. The dotted lines give the errors calculated with minimum (e) and maximum (f) absorption thicknesses, respectively. The effect of x-ray-absorption fine structure on the total efficiency (a) is not visible at this scale. (b) Detection efficiency for four different measurements at $\Phi = 0.04$ (a, full line), $\Phi = 1.0$ (g, dashed line), $\Phi = 0.01$ (h, dotted line), $\Phi = 0.08$ (i, dashed-dotted line). The difference is mainly due to the different thicknesses of the target cell windows for the respective setups.

directly or estimated by simulation.

To show the various contributions to the calculated error of the detection efficiency, we use again the example of the measurement at 4% of LHD, where $\eta(K\alpha)/\eta(K\beta) = 0.413 \pm 0.058$. The relative error of this efficiency ratio of $\sim 14\%$ is the sum of the following uncertainties: (i) 8.1% (Kapton and Hostaphan windows), (ii) 4.0% (x-ray absorption coefficients), (iii) 1.8% (thickness of CCD absorption layers), (iv) 0.04% (path length in deuterium of 4% of LHD), (v) 0.006% (deuterium density). These numbers vary for the different measurements. As some of the contributions are not fully independent in terms of statistics, we conservatively estimate the total error by adding them linearly.

B. Analysis of the energy spectra

The measured energy spectra were analyzed by fitting Gaussians with energy-dependent widths to the individual lines [18,40,41,44]. The background was approximated by a constant and a term depending linearly on energy. The peak at 1.74 keV was due to fluorescence of the detector's silicon material. Its position and width are very well known and the line can be accurately approximated by a Gaussian.

In a μ^+ run we observed the shape of the background due to bremsstrahlung. An additional empty target run proved that no other background peaks were visible in the relevant energy region.

The line intensities were corrected with the calculated detection efficiency. From the corrected intensities two quantities were evaluated: (i) The relative yield of each K line, which is given by the intensity of this K line (K_i, $i = \alpha, \beta, \gamma$) divided by the sum of the intensities of all observed K lines ($K_{tot} = \Sigma_i K_i$); (ii) the $K\alpha/K\beta$ ratio (K ratio). (Intensity of the $K\alpha$ line divided by the intensity of the $K\beta$ line.)

C. Results in D_2

Our results for the relative x-ray yields and the $K\alpha/K\beta$ ratio in muonic deuterium are given in Table I. Figure 4 compares the relative yields with the new calculations of Aschenauer and Markushin [6] in terms of different scaling factors k for Coulomb deexcitation (see Sec. II): $k = 0$ means no relevant contribution from this process; $k = 1$ means the cross sections of Bracci and Fiorentini [24] are correct. In the density region investigated, the calculations predict the relative yield and its density dependence to depend significantly on the contribution of Coulomb deexcitation (Fig. 4). A strong, approximately linear dependence on density is predicted for the $K\alpha/K\beta$ ratio, as seen in Fig. 5.

In Fig. 4, the displayed data point at LHD includes a 5% correction due to collisionally induced transitions to the ground state, according to [6]. These transitions cannot be observed by our x-ray detector. This correction is necessary

TABLE I. Results of the muonic x-ray measurements in deuterium. T indicates the target temperature in K. The given experimental errors include statistical errors and contributions due to uncertainties in the efficiency correction.

Density (LHD)	T (K)	$K\alpha/K_{tot}$	$K\beta/K_{tot}$	$K\gamma/K_{tot}$	$K\alpha/K\beta$
1.145±0.0060	23.8±0.1	0.953±0.025	0.047±0.010	0.0±0.002	20.3±2.7
1.142±0.0030	24.0±0.1	0.954±0.015	0.046±0.006	0.0±0.002	20.6±2.2
0.0783±0.0007	31.5±0.2	0.829±0.029	0.156±0.026	0.016±0.004	5.32±1.27
0.0751±0.0007	31.7±0.2	0.826±0.033	0.157±0.027	0.018±0.007	5.27±0.90
0.0613±0.0003	30.6±0.2	0.788±0.040	0.190±0.033	0.022±0.013	4.15±0.78
0.0560±0.0005	31.2±0.2	0.794±0.040	0.184±0.032	0.022±0.011	4.31±0.74
0.0399±0.0003	28.0±0.2	0.685±0.035	0.275±0.029	0.040±0.007	2.49±0.35
0.0133±0.0001	27.1±0.2	0.538±0.042	0.365±0.031	0.097±0.014	1.48±0.22
0.0107±0.0001	30.3±0.2	0.568±0.062	0.345±0.056	0.086±0.029	1.65±0.30

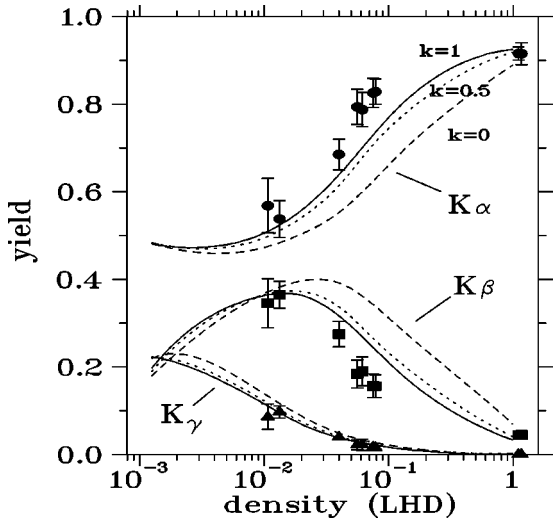

FIG. 4. The density dependence of the yield of muonic K lines in deuterium. The experimental value of the relative yield is given as the number of counts in one K line (K_i, $i=\alpha,\ \beta,\ \gamma$) divided by the total count rate in all observed K lines ($K_{\mathrm{tot}}=\Sigma_i K_i$). The plotted data points at LHD include a 5% correction due to collisionally induced transitions to the ground state [6]. Filled circles, squares, and triangles indicate the relative yields for $K\alpha$, $K\beta$, and $K\gamma$ transitions, respectively. Our results are compared with the calculated density dependence calculated by Aschenauer and Markushin [6] for different scaling factors $k=0$ (dashed line), $k=0.5$ (dotted line), and $k=1$ (solid line).

only at LHD and only to compare the measured ''relative'' yield with the ''absolute'' yield given in the calculation. One could also use our definition of the relative yield and extract the relevant values from the calculation, in which case we would not have to correct the measured values. No correction was applied for the gas measurements because ground-state transitions are expected to be purely radiative at the gas densities investigated.

Regarding the x-ray yield, the observed density dependence is reproduced quite well by theory. The experimental

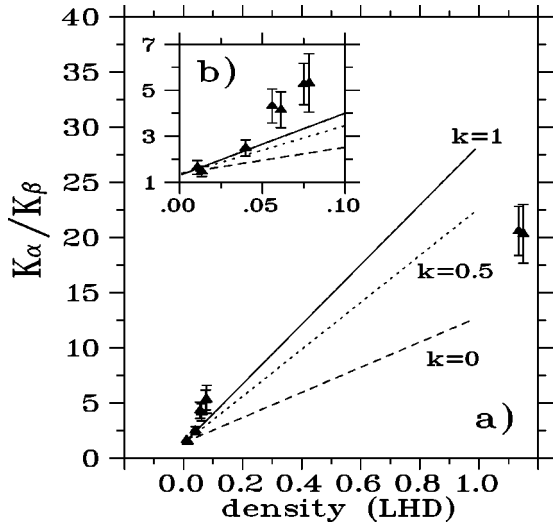

FIG. 5. (a) The density dependence of the $K\alpha/K\beta$ ratio measured in muonic deuterium (filled triangles). The theoretical curves are the calculations of Aschenauer and Markushin [6] (see Fig. 4). (b) The low-density region magnified.

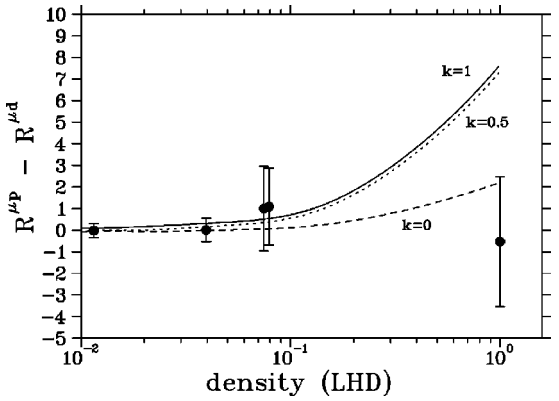

FIG. 6. The density dependence of the difference between the $K\alpha/K\beta$ ratios of muonic hydrogen and deuterium ($R^{\mu p}-R^{\mu d}$). Our experimental points (filled dots) are compared to the calculation of Aschenauer and Markushin [6]. The lines are interpolations for $k=0$ (dashed line), $k=0.5$ (dotted line), and $k=1$ (solid line).

errors include statistical errors and contributions due to uncertainties in the efficiency correction. Although the yield measurement is not very sensitive to k within the experimental errors, it favors values of $k\approx 1$. An even higher contribution of Coulomb deexcitation is suggested by our data at densities around 8% of LHD.

In Fig. 5 our results for the $K\alpha/K\beta$ ratios are displayed together with calculation [6]. The data at LHD favor a scaling factor between 0.1 and 0.5, however the data at $\sim 4\%$ and $\sim 8\%$ of LHD are higher than expected by theory. Although each of these points has a large error bar, together they indicate a significant deviation from the $k=1$ calculation.

Comparing all our experimental results in deuterium with theory, they indicate an important contribution of Coulomb deexcitation to the muonic cascade. An unambiguous determination of the correct value of the scaling factor k is not possible. In fact, the Monte Carlo cascade model cannot reproduce the density dependence of our data by simply scaling the Coulomb deexcitation cross sections from [24]. This clear indication of a more complex density dependence could be due to possible new processes, for example, the existence of molecular effects [57,58].

D. Comparison of results in D_2, H_2, and hydrogen deuterium mixtures

We can compare our measurements in D_2 and H_2 [8] in search of an isotopic effect. We do not observe any difference for either the K yield or the $K\alpha/K\beta$ ratio. Comparing the density dependence of the K yield of muonic deuterium (Fig. 4) and muonic hydrogen [8], one can see a comparable systematic deviation from the theoretical expectation [6] but no isotopic difference. This is also true for the experimental values of the $K\alpha/K\beta$ ratios (Fig. 5 and Ref. [8]).

A direct quantity for expressing the isotopic difference between the $K\alpha/K\beta$ ratios can be defined as $R^{\mu p}-R^{\mu d}$; ($R^{\mu p}=K_\alpha^{\mu p}/K_\beta^{\mu p}$ in muonic hydrogen [8], $R^{\mu d}=K_\alpha^{\mu d}/K_\beta^{\mu d}$ in muonic deuterium). The calculation derived from Ref. [6] predicts an ($R^{\mu p}-R^{\mu d}$) dependence on density, different for varying contributions of Coulomb deexcitation to the cascade. As can be seen in Fig. 6, the cal-

culation is rather insensitive to varying contributions of Coulomb deexcitation at gas densities, but a clear difference for different scaling factors k exists at LHD. However, the experimental values do not display a dependence on density over the whole range of measurements from $\sim 1\%$ to $\sim 100\%$ of LHD. The experimental point at LHD clearly favors the assumption $k=0$. (For this evaluation we have neglected the difference in density for liquid H_2 and D_2.)

Additional measurements of the radiative transitions in the density region between 10% and 100% of LHD could shed light on the actual density dependence and on the accurate contribution of Coulomb deexcitation. Such measurements have not been done yet as they require a very strong material for the thin target windows which presently does not exist. Current high pressure target windows absorb too many x rays to permit a statistically significant observation of 2 keV x rays.

Measurements of the muonic cascade in tritium would also be desirable to see if there is a difference in the $K\alpha/K\beta$ ratio compared to that in hydrogen or deuterium.

In addition to isotopically pure targets, we have measured the dependence on the deuterium concentration of the line yields and the $K\alpha/K\beta$ ratio in liquid hydrogen deuterium mixtures. This density was chosen because theory expects the largest isotopic difference ($\sim 20\%$) for the $K\alpha/K\beta$ ratio at liquid density.

In mixtures of hydrogen isotopes one has to take into account one additional cascade process, the transfer of the muon in excited states [18,35,45,59], which changes the intensity pattern of the K lines observed at each isotope. This transfer is expected to proceed between isotopic states of the same principal quantum number and does not lead to cascade deexcitation. Therefore, the total yield, given for the $K\alpha$ line by $\Sigma_{K\alpha}=K_\alpha^{\mu p}+K_\alpha^{\mu d}$ or for the $K\beta$ line by $\Sigma_{K\beta}=K_\beta^{\mu p}+K_\beta^{\mu d}$, divided by $\Sigma_{K\mathrm{tot}}=K_{\mathrm{tot}}^{\mu p}+K_{\mathrm{tot}}^{\mu d}$, respectively, should be independent of the excited state transfer process.

Assuming the same importance of Coulomb deexcitation in the cascade of muonic hydrogen and muonic deuterium at LHD, one expects an isotopic effect for the $\Sigma_{K\alpha}$ yield [Fig. 7(a)] of only $\sim 1\%$, for the $\Sigma_{K\beta}$ yield [Fig. 7(b)] of more than $\sim 10\%$ and for the $\Sigma_{K\alpha}/\Sigma_{K\beta}$ ratio (Fig. 8) of ~ 15–25%, for a given value of k.

As a result of these measurements, given in Table II, one can state that the intensity pattern of the sum of the relative intensities of the respective K lines (total yield) does not depend on deuterium concentration. Again, no isotopic difference between deuterium and hydrogen, neither for the total yield nor for the $\Sigma_{K\alpha}/\Sigma_{K\beta}$ ratio has been observed.

In Figs. 7 and 8 these results are compared with the calculations from Refs. [6,34]. There the parameters $k=0.5$ and $k_t=0.5$ (scaling factor for the excited state transfer cross sections) were selected for the best fit of the q_{1s} parameter (Refs. [18,35]) in hydrogen deuterium mixtures. Our measurements deviate from this prediction, although one has to keep in mind the large experimental errors in comparison to the expected effect.

From our measurements at LHD we can derive that the probability for radiative deexcitation at the levels $n=2$ and $n=3$ is equal for D_2 and H_2 within the experimental errors. We have not observed an isotopic effect in the competition between collisional processes and x-ray emission at the $n=3$ level.

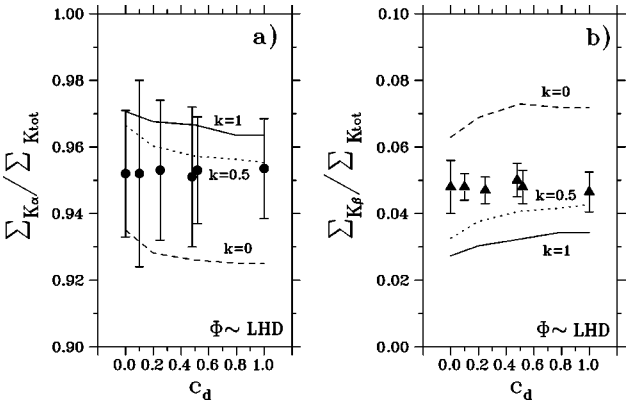

FIG. 7. The dependence of the (a) total $K\alpha$ yield and (b) total $K\beta$ yield on the deuterium concentration in liquid-hydrogen deuterium mixtures. Our measurements (filled dots and triangles) are compared to the theoretical expectation taken from [6,34] for the Coulomb deexcitation scaling factors $k=0$ (dashed line), $k=0.5$ (dotted line), and $k=1$ (full line). There is no dependence on k_t, the scaling factor of the excited state transfer cross sections expected. Note the different ranges on the y axis of (a) and (b).

Besides our measurement at $c_d=0.5$ in a nonequilibrated hydrogen deuterium mixture (50% H_2 molecules, 50% D_2 molecules), we have also investigated a hydrogen deuterium mixture at $c_d=0.5$ in molecular equilibrium (equilibrated mixture: 25% H_2 molecules, 50% HD molecules, 25% D_2 molecules), both as liquids. The molecular composition of the target was carefully determined with the mass spectrometer (QMS) at the beginning, during, and at the end of this measurement. From the equality of these two measurements we conclude that there are no effects larger than 10% due to the different isotopic composition of the molecules involved in the collisional deexcitation.

In conclusion, we find that scaling the Coulomb deexcitation cross sections is not enough to reproduce our measure-

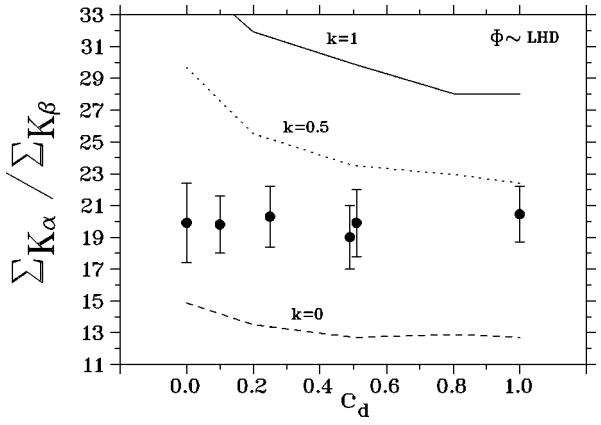

FIG. 8. The dependence of the $\Sigma_{K\alpha}/\Sigma_{K\beta}$ ratio on the deuterium concentration in liquid-hydrogen deuterium mixtures. Our experimental points (filled dots) are compared to the theoretical expectation taken from [6,34] for scaling factors $k=0$ (dashed line), $k=0.5$ (dotted line), and $k=1$ (full line). No dependence on k_t, the scaling factor of the excited-state transfer cross sections, is expected.

TABLE II. Results of the muonic x-ray measurements in liquid hydrogen [8] and liquid H_2/D_2 mixtures. c_d indicates the deuterium concentration in the isotopic mixture. The given experimental errors include statistical errors and contributions due to uncertainties in the efficiency correction.

Density (LHD)	T (K)	c_d	$\Sigma_{K\alpha}/\Sigma_{Ktot}$	$\Sigma_{K\beta}/\Sigma_{Ktot}$	$\Sigma_{K\alpha}/\Sigma_{K\beta}$
0.970±0.005	22.1±0.1	0.000±0.001	0.952±0.019	0.048±0.008	19.9±2.5
0.979±0.003	22.7±0.1	0.099±0.004	0.952±0.028	0.048±0.004	19.8±1.8
1.035±0.005	21.3±0.1	0.247±0.006	0.953±0.021	0.047±0.004	20.3±1.9
1.075±0.005	21.9±0.1	0.499±0.008	0.951±0.021	0.050±0.005	19.0±2.0
1.070±0.005[a]	22.1±0.1	0.500±0.008	0.953±0.016	0.048±0.005	19.9±2.1

[a]While all the other mixtures contain practically only H_2 and D_2 molecules, this is an equilibrated mixture having 25% H_2, 50% HD, and 25% D_2 molecules.

ments by a cascade calculation. The large variation of the scaling factor describing the measurements in Figs. 4–8 indicates that, in the Monte Carlo cascade calculation [6] at least, the Coulomb deexcitation cross sections and their density dependence are wrong, or, that not all cascade processes were taken into account. Both possibilities definitely call for an improved theoretical treatment.

New results from PSI concerning the K yields in H_2 and D_2 at very low gas densities ($\Phi<0.1\%$ of LHD) [60] will complement our investigations.

Experiments measuring the x rays in pionic hydrogen and deuterium [61] have found an isotopic effect for the $K\alpha$ yield at a pressure of 40 bar ($\sim 5\%$ of LHD). Regarding the pionic cascade in hydrogen and deuterium, a fair agreement between theory and experiment could be obtained by employing a Coulomb deexcitation scaling factor $k=0.5\pm0.2$. This value of k also fits the results obtained by neutron time-of-flight measurements after pion capture in hydrogen [62].

But additional uncertainties in pionic hydrogen and deuterium due to the inexact knowledge of the Stark mixing rates and of the nuclear absorption complicate the determination of the cascade parameters. Therefore the comparison with the muonic case is an important constraint for the Coulomb deexcitation rates.

V. SUMMARY

We have performed a systematic investigation of the muonic cascade in deuterium and searched for an isotopic effect in comparison with our measurements in hydrogen and in liquid hydrogen deuterium mixtures, thus providing an accurate database for the K yields and the $K\alpha/K\beta$ ratios. These data allow a detailed comparison with recent calculations, which treat the Coulomb deexcitation rates as an adjustable parameter. Our detailed data cannot be consistently explained by scaling one model parameter only. In particular, we observe (i) a density dependence of the K yield and the $K\alpha/K\beta$ ratio different from theoretical expectation, (ii) no isotopic difference for the line yields and the $K\alpha/K\beta$ ratios, in contrast to theory.

We would like to stimulate improved calculations of the cross sections of the various cascade processes which could then be included in an improved cascade simulation.

ACKNOWLEDGMENTS

Financial support by the Austrian Science Foundation, the Austrian Academy of Sciences, the Swiss Academy of Sciences, the Swiss National Science Foundation, and the German Federal Ministry of Research and Technology is gratefully acknowledged. It is a pleasure to thank D. Sigg for his software support and D. Varidel for his excellent technical assistance. Many fruitful discussions with E.C. Aschenauer, V.E. Markushin, and M.P. Faifman are acknowledged. Finally, we gratefully thank R. King for his criticism and corrections.

[1] M. Leon and H. A. Bethe, Phys. Rev. **127**, 636 (1962).
[2] M. Leon, Phys. Lett. **35B**, 413 (1971).
[3] V. E. Markushin, Zh. Éksp. Teor. Fiz. **80**, 35 (1981) [Sov. Phys. JETP **53**, 60 (1981)].
[4] V. E. Markushin, in *Electromagnetic Cascade and Chemistry of Exotic Atoms*, edited by L. M. Simons, D. Horvath, and G. Torelli (Plenum, New York, 1989), p. 73.
[5] V. E. Markushin, Phys. Rev. A **50**, 1137 (1994).
[6] E. C. Aschenauer and V. E. Markushin, Hyperfine Interact. **101/102**, 97 (1996); Z. Phys. D **39**, 165 (1997).
[7] F. Kottmann, in *Muonic Atoms and Molecules*, edited by L. A. Schaller and C. Petitjean (Birkhäuser, Basel, 1993), p. 219.
[8] B. Lauss *et al.*, Phys. Rev. Lett. **80**, 3041 (1998).
[9] A. Placci *et al.*, Phys. Lett. **32B**, 413 (1970).
[10] B. Budick *et al.*, Phys. Lett. **34B**, 539 (1971).
[11] H. Anderhub *et al.*, Phys. Lett. **71B**, 443 (1977).
[12] P. O. Egan *et al.*, Phys. Rev. A **23**, 1152 (1981).
[13] H. Anderhub *et al.*, Phys. Lett. **143B**, 65 (1984).
[14] W. H. Breunlich, P. Kammel, J. S. Cohen, and M. Leon, Annu. Rev. Nucl. Part. Sci. **39**, 311 (1989).
[15] J. Zmeskal *et al.*, Phys. Rev. A **42**, 1165 (1990).
[16] P. Kammel, Lett. Nuovo Cimento **43**, 349 (1985).
[17] M. Jeitler *et al.*, Phys. Rev. A **51**, 2881 (1995).
[18] B. Lauss *et al.*, Phys. Rev. Lett. **76**, 4693 (1996).
[19] D. Chatellard *et al.*, Nucl. Phys. A **625**, 855 (1997); Phys. Rev. Lett. **74**, 4157 (1995).
[20] G. C. Oades *et al.*, Proposal R-98-01.1, Paul Scherrer Institut, Switzerland, 1998.

[21] J. S. Cohen, R. L. Martin, and W. R. Wadt, Phys. Rev. A **27**, 1821 (1983).
[22] G. A. Fesenko and G. Ya. Korenman, Hyperfine Interact. **101/102**, 91 (1996).
[23] W. H. Breunlich, Nucl. Phys. A **335**, 137 (1980).
[24] L. Bracci and G. Fiorentini, Nuovo Cimento A **43**, 9 (1978).
[25] E. C. Aschenauer *et al.*, Phys. Rev. A **51**, 1965 (1995).
[26] F. J. Hartmann *et al.*, Hyperfine Interact. **101/102**, 623 (1996).
[27] F. J. Hartmann *et al.*, PSI Annual Report 1996, Annex I, p. 31.
[28] L. I. Men'shĭkov, Muon Catal. Fusion **2**, 173 (1988).
[29] A. V. Kravtsov and A. I. Mikhaĭlov , Zh. Éksp. Teor. Fiz. **107**, 1473 (1995) [Sov. Phys. JETP **80**, 822 (1995)]; Nukleonika **40**, 25 (1995).
[30] W. Czaplinski *et al.*, Phys. Rev. A **50**, 525 (1995).
[31] L. I. Ponomarev and E. V. Solov'ev, Pis'ma Zh. Éksp. Teor. Fiz. **64**, 140 (1996) [JETP Lett. **64**, 135 (1996)].
[32] T. B. Day *et al.*, Phys. Rev. **118**, 864 (1960).
[33] E. Borie and M. Leon, Phys. Rev. A **21**, 1460 (1980).
[34] E. C. Aschenauer and V. E. Markushin (private communication).
[35] B. Lauss *et al.*, Hyperfine Interact. **101/102**, 285 (1996).
[36] S. S. Gershteĭn, Zh. Éksp. Teor. Fiz. **43**, 706 (1962) [Sov. Phys. JETP **16**, 501 (1963)].
[37] B. Gartner, Diploma thesis, University of Graz, 1994 (unpublished).
[38] D. Varidel *et al.*, Nucl. Instrum. Methods Phys. Res. A **292**, 141 (1990).
[39] G. Fiorucci *et al.*, Nucl. Instrum. Methods Phys. Res. A **292**, 147 (1990).
[40] J.-P. Egger, D. Chatellard, and E. Jeannet, in *Muonic Atoms and Molecules*, (Ref. [7]), p. 331.
[41] J.-P. Egger, D. Chatellard, and E. Jeannet, Part. World **3**, 139 (1993).
[42] D. Chatellard, Ph.D. thesis, University of Neuchâtel, 1995 (unpublished).
[43] D. Sigg, Nucl. Instrum. Methods Phys. Res. A **345**, 107 (1994).
[44] B. Lauss, Ph.D. thesis, University of Vienna, 1997 (unpublished).
[45] B. Lauss *et al.*, in *Proceedings of the LEMS'93 Workshop, Los Alamos*, LA-12698 C (Los Alamos National Laboratory, Los Alamos, 1993), p. 300.
[46] Fortran Code Space93, B. Lauss, IMEP/ÖAW-1993/94.
[47] GEANT – *Detector Description and Simulation Tool*, CERN Program Library W5013.
[48] English Electric Valve (EEV) (private communication).
[49] S. I. Salem, S. L. Panossian, and R. A. Krause, At. Data Nucl. Data Tables **14**, 91 (1974).
[50] D. Anagnostopoulos *et al.*, Phys. At. Nucl. **59**, 1503 (1996).
[51] R. Bacher *et al.*, Phys. Rev. A **38**, 4395 (1988).
[52] B. L. Henke, E. M. Gullikson, and J. C. Davies, At. Data Nucl. Data Tables **54**, 181 (1993), and http://xray.uu.se/hypertext/henke.html
[53] G. W. Fraser *et al.*, Nucl. Instrum. Methods Phys. Res. A **350**, 368 (1994).
[54] A. Owens *et al.*, Nucl. Instrum. Methods Phys. Res. A **382**, 503 (1995).
[55] E. Storm and H. Israel, At. Data Nucl. Data Tables **7**, 565 (1970).
[56] J. H. Hubbell, Int. J. Appl. Radiat. Isot. **33**, 1269 (1982).
[57] P. Froelich and J. Wallenius, Phys. Rev. Lett. **75**, 2108 (1995).
[58] D. Taqqu, in *Muon-Catalyzed Fusion, Proceedings of the $\mu CF'88$ Meeting, Sanibel Island*, edited by Steven E. Jones, Hohann Rafelski, and Hendrick J. Monkhorst, AIP Conf. Proc. No. 181 (AIP, New York, 1988), p. 217.
[59] L. I. Menshikov and L. I. Ponomarev, Pis'ma Zh. Éksp. Teor. Fiz. **42**, 12 (1985) [JETP Lett. **42**, 13 (1985)].
[60] M. Bregant *et al.*, Phys. Lett. A **241**, 344 (1998).
[61] A. J. Rusi El Hassani *et al.*, Z. Phys. A **351**, 113 (1995).
[62] E. C. Aschenauer *et al.*, Phys. Rev. A **51**, 1965 (1995).